Int. J. Heat Mass Transfer. Vol. 35, No. 12, pp. 3363–3374, 1992
Printed in Great Britain

0017 9310/92 $5.00 + 0.00

Entrance region heat transfer in a channel downstream of an impinging jet array

ALOK SARKAR† and L. W. FLORSCHUETZ
Department of Mechanical and Aerospace Engineering, Arizona State University, Tempe, AZ 85287-7106, U.S.A.

(*Received* 22 *April* 1991 *and in final form* 10 *January* 1992)

Abstract—An experimental investigation is carried out on the entrance region heat transfer in a parallel plate channel downstream of a jet array located in one of the plates. The jet impingement surface is kept isothermal while the opposing surface, containing the jet array, is adiabatic. The focus of the investigation is the systematic study of the effect of flow rate and array geometric parameters on local Nusselt numbers in the entrance region of the channel immediately downstream of the array. To place these results in context, Nusselt numbers opposite the array and in the fully developed region downstream of the channel entrance are also included. In the entrance region, the ratio of the local to fully developed Nusselt number is independent of the channel Reynolds number, and the effects of some jet array geometric parameters are significant. These effects become negligible within 10 hydraulic diameters from the channel entrance. The entrance length is about 21 hydraulic diameters. The fully developed Nusselt numbers agree well with previous measurements. Empirical correlations are developed to fit the observations.

INTRODUCTION

IMPINGEMENT with high velocity gas jets has become an established method of convectively cooling or heating surfaces in a wide variety of processes and thermal control applications. The advantages of this method are twofold: the high heat transfer coefficients for given flow rates, and the possibility to closely obtain a desired spatial distribution of heat transfer rates through different geometric arrangements of multiple jets. Examples include cooling of gas turbine airfoils and electronic equipment, drying of paper and textiles or other thin films, annealing of metals and glass tempering operations. The present study is motivated by possible applications in the cooling of midchord regions of current and contemplated airfoils. One possible arrangement has an inlet plenum inside the hollowed out midchord region of an airfoil. Through holes drilled on the two flanks of the inlet plenum coolant jets impinge on the inside surface of the airfoil. There may be additional rows of jets on the leading edge of the plenum to help cool the tip of the airfoil. The geometry of the airfoil application dictates that all of the jet flow will exit in the chordwise direction towards the trailing edge. Consequently the exhaust from the upstream jets imposes a crossflow on the downstream jets. For one rather detailed example of this configuration see Gauntner *et al.* [1].

This combination of jet array impingement with one sided exhaust has stimulated a number of experimental studies in convective heat transfer. Dyban *et al.* [2], Florschuetz *et al.* [3, 4], Florschuetz and Tseng [5], Goldstein and Timmers [6], Kercher and Tabakoff [7] and Metzger *et al.* [8] studied heat transfer rates directly under arrays of impinging jets over different ranges of geometric and flow parameters. Florschuetz *et al.* [9] and Florschuetz and Su [10] studied the effects of an initial crossflow, and its temperature on the heat transfer coefficients under the jet array. There also had been some studies on interaction between a single jet and a crossflow, with more emphasis on details of the flowfield, e.g. Bouchez and Goldstein [11], Ramsey and Goldstein [12] and Sparrow *et al.* [13].

All the studies involving jet array impingement concentrated on heat transfer rates directly under the jet array. In practice heat transfer rates downstream of the jet array, or in other words the entrance region heat transfer in the channel downstream of the jet array, is of interest too. Its knowledge will be crucial in deciding the optimum cooling arrangements in situations involving nonuniform thermal loads. Entrance region heat transfer in special geometries can be quantitatively very different from that in a straight parallel channel, e.g. Sparrow and Kemink [14], Sparrow and Cur [15]. These two papers indicate the importance of detailed experimental study of the problem described above. The present paper reports the results of such a study. Though the above discussion emphasized possible applications in cooling of gas turbine airfoils, the present experiments are general enough to have much wider applicability.

PROBLEM FORMULATION

Figure 1 defines the geometry, the coordinate system and the geometric nomenclature. The proper set

† Present address: Department of Geology and Geophysics, Louisiana State University, Baton Rouge, LA 70803 U.S.A.

NOMENCLATURE

c_p	specific heat of air at constant pressure
d	jet hole diameter (Fig. 1)
h	heat transfer coefficient (equation (4))
I	denotes 'inline' jet hole array pattern, e.g. (5, 4, 3, 4)I (Fig. 1)
k	thermal conductivity of air
n	test plate segment number
Nr	number of transverse jet rows (Fig. 1)
Nu	transverse average Nusselt number, $h(2z_n)/k$
Pr	Prandtl number
$q(x^+)$	transverse averaged heat flux
Re	channel Reynolds number based on channel flow rate and hydraulic diameter
Re_j	jet Reynolds number, $\rho V_j d/\mu$
S	denotes 'staggered' jet hole array pattern, e.g. (5, 4, 3, 4)S (Fig. 1)
Sc	Schmidt number
Sh	Sherwood number
$T_r(x^+)$	fluid reference temperature; under the jet array defined as jet exit total temperature; in the channel defined as the local mixed mean total temperature
T_w	isothermal temperature of the test surface
V_c	mean crossflow velocity approaching downstream transverse jet row (at $x = 0$, Fig. 1)
V_j	mean jet exit velocity
x_n	streamwise jet hole spacing (Fig. 1)
x^+	nondimensional streamwise coordinate, $x/2z_n$
y_n	transverse jet hole spacing (Fig. 1)
z_n	channel depth (Fig. 1)
z^+	nondimensional vertical coordinate, z/z_n.

Greek symbols

ε	heat flux at zero reference temperature difference
μ	dynamic viscosity of air
ρ	density of air.

Subscript

∞	fully developed value in channel.

of nondimensional parameters was identified from the governing equations and boundary conditions, as would be encountered in a purely theoretical formulation of the present heat transfer problem. High velocity effects such as interchange of thermal and mechanical energies and viscous dissipation can be significant for jet impingement heat transfer [10, 16]. Therefore, the problem was treated as a constant property high velocity flow. The problem was formulated in terms of total temperature, instead of static temperature, as it is convenient in high velocity flows. It was also taken into account that, because of the presence of the crossflow of spent air the jet exit velocity would vary from row to row. It was concluded that the transverse averaged Nusselt number in the channel downstream of the jet array would be a function of the following parameters:

$$\{x/2z_n, x_n/d, y_n/d, z_n/d, Nr, Re, Pr\}. \quad (1)$$

The analysis also indicated that the transverse averaged heat flux at the lower surface may be expressed as

$$q(x^+) = h(x^+)[T_w - T_r(x^+)] + \varepsilon(x^+) \quad (2)$$

where $\varepsilon(x^+)$ is the heat flux at zero reference temperature difference, which is in general nonzero because of the presence of recovery effects and viscous dissipation. $h(x^+)$ is the transverse averaged heat transfer coefficient. Under the jet array, the fluid reference temperature, $T_r(x^+)$, was taken to be the total temperature at the jet exit equivalent to the jet plenum temperature, while in the channel downstream of the array it was defined as the mixed mean total temperature.

The implication of equation (2) is that to determine the heat transfer coefficient one has to take measurements for at least two non-zero power input levels, as the adiabatic surface would not necessarily be iso-

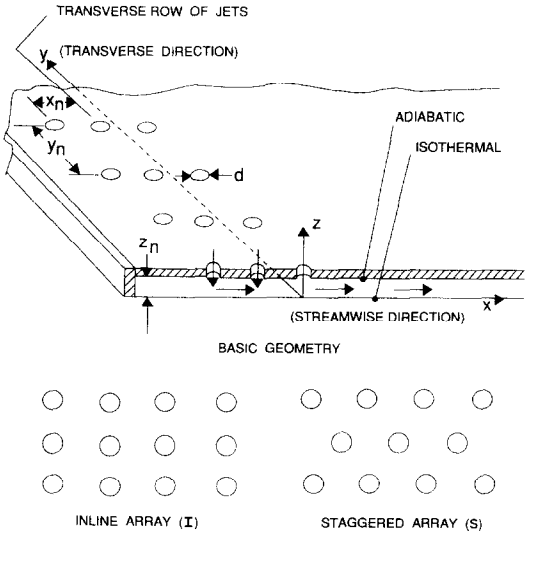

FIG. 1. Definition geometry and coordinate system.

thermal, and then take the slope of the heat flux vs $T_w - T_r$ plot. The advantage of equation (2) is that the relationship between $Nu(x^+)$, Re and Pr will be applicable even for low velocity flows. Because recovery effects, reflected by the term $\varepsilon(x^+)$ in equation (2), were typically quite small, experimental uncertainties for recovery factors were relatively large. Therefore, recovery effects are not reported. For details of the analysis please refer to Sarkar [17].

During experiments the maximum temperature difference ever encountered was 30 K. To obtain results corresponding to constant property analysis, the effects of streamwise and depthwise variations of fluid temperature were accounted for during data reduction. The channel Mach number was always less than 0.2. The jet Mach number varied mostly between 0.2 and 0.6. This may suggest including jet Mach number as an important parameter. Theoretical analysis indicates that under the assumption that Pr, $(\rho\mu)$ and c_p are constant and the normal pressure gradients at the heat transfer surface vanish, the relationships between $Nu(x^+)$, Re and Pr are the same for both constant and variable property, high velocity heat transfer problems [18]. All the above conditions are very closely satisfied in the present set of experiments. Also the primary interest here is in the channel where the flow is incompressible. Hence jet Mach number was not considered to be an important parameter.

EXPERIMENTAL FACILITY

The test facility consisted of a compressed air supply, an air flow metering section and interchangeable plenum/jet plate assemblies, which produced arrays of jets impinging on an instrumented heat transfer test surface. The test surface and a parallel extension plate extended beyond the jet array in the direction of exhaust of the spent air, and constituted a parallel plate channel. Subsequent to impingement the spent air flowed through the channel to exhaust into the free atmosphere. The streamwise and transverse cross sectional views of the assembly are shown in Fig. 2. The present setup is a modification of the facility used by Florschuetz and Su [10].

A single test plate unit consisting of a segmented copper test plate with individual segment heaters, the necessary thermal insulation and the test plate support structure was used for all tests. The jet array exit plane and the extension plate were positioned relative to heat transfer surface via interchangeable spacers to vary the channel height. The uniformity of the flow upstream of the jet plate was ensured by passing laboratory air through the plenum packing. The plenum air temperature and pressure were monitored continuously. Subsequent to impingement on the test plate, the air exhausted to atmospheric pressure by flowing along the channel formed by the jet plate and the extension plate, the test surface and the spacer.

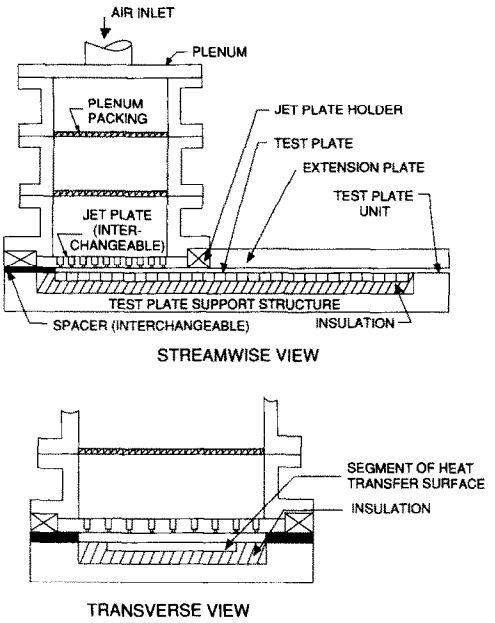

FIG. 2. Sectional views of test rig.

These components are shown in assembled form in Fig. 2.

Each jet plate had 10 transverse rows of holes, each row centered directly over one of the first 10 copper segments of the test plate. The maximum streamwise resolution for determination of heat transfer coefficients was equal to one streamwise hole spacing x_n. The maximum active streamwise length of the test plate was 38.1 cm (15 in.) (30 segments by 1.27 cm per segment, with an additional segment at the downstream end to serve as a guard heater). The transverse width of the test plate and the channel were fixed at 12.2 cm (4.8 in.) and 18.3 cm (7.2 in.), respectively. The excess width of the channel permitted the jet hole pattern to extend beyond the edges of the heat transfer surface, thus minimizing flow pattern edge effects on the heat transfer characteristics (see Fig. 2, transverse view). The active instrumented part of the test plate extended beyond the last transverse jet row in the streamwise direction by 25.4 cm (10 in.). The additional length was covered at the top by the plexiglass extension plate. The duct under the extension was the main part of the channel. The beginning of the channel was assumed to be from the imaginary plane passing through the centerline of the last transverse jet row.

To obtain the number of transverse rows required for a given test, unneeded rows were blocked by a few layers of adhesive tape on the plenum side. To eliminate the possibility of any flow distortion resulting from inactive jet holes, which appeared as indentations on the channel side of the jet plate, they were always kept upstream of the impinging jet rows.

The copper test plate segments were 0.64 cm (1/4 in.) thick and 1.19 cm (15/32 in.) wide, with 0.079

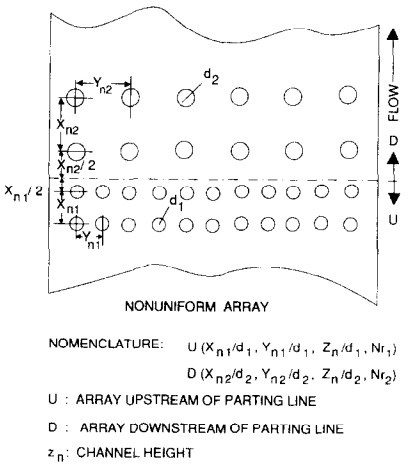

FIG. 3. Nonuniform jet hole pattern.

cm (1/32 in.) balsa wood insulation bonded between adjacent segments to minimize heat leakage. The individual heaters were foil type bonded to the underside of each segment, each with power input controlled by a separate variac. The primary temperature instrumentation in the test plate consisted of a copper–constantan thermocouple mounted in the center of each copper segment, with a redundant thermocouple in each segment offset by 1.52 cm (0.6 in.) in the spanwise direction. Several segments had additional thermocouples to monitor spanwise temperature distributions. To ensure smoothness of the test surface in spite of its segmented construction, it was resurfaced after assembly.

In this paper a given geometry will be referred to by the notation: $(x_n/d, y_n/d, z_n/d, Nr)$I (or S). For example (5, 4, 3, 2)I will mean $x_n/d = 5$, $y_n/d = 4$, $z_n/d = 3$, $Nr = 2$ with I indicating an 'inline' hole pattern. Jet plates with an inline hole pattern had holes located at the intersection points of an uniform rectangular grid. An S at the end of the parentheses indicates a 'staggered' hole pattern, in which alternate transverse rows are offset by one-half the transverse hole spacing (Fig. 1). In the case of nonuniform hole patterns, the test plate was divided into two regions parallel to the transverse direction, each region with a different inline hole pattern (Fig. 3). A designer may consider using staggered jet array geometries to avoid local hot spots, or a nonuniform array to match a spatially variable cooling load. Hence these array geometries were included in the study. Table 1 summarizes the geometries and flow rates for which tests were run.

Table 1. Geometries and flow rates tested†

Geometry	$Re \times 10^{-3}$
Inline array	
(5, 4, 1, 1)I	10.3
(5, 4, 1, 2)I	10.5
(5, 4, 1, 4)I	10.1
(5, 4, 3, 1)I	10.2
(5, 4, 3, 4)I	10.3
(5, 8, 1, 1)I	3.0
(5, 8, 1, 1)I	8.0
(5, 8, 1, 4)I	10.2
(5, 8, 2, 2)I	13.4
(5, 8, 3, 1)I	7.8
(5, 8, 3, 4)I	10.3
(10, 4, 1, 1)I	7.3
(10, 4, 3, 1)I	8.1
(10, 4, 3, 2)I	9.9
(10, 4, 3, 4)I	10.0
(10, 4, 3, 5)I	10.0
(10, 4, 3, 5)I	13.0
(10, 4, 3, 5)I	18.4
(10, 4, 3, 5)I	18.6
(10, 8, 1, 4)I	10.2
(10, 8, 3, 4)I	10.0
(10, 8, 6, 4)I	10.1
Staggered array	
(5, 4, 3, 4)S	9.9
(5, 8, 2, 2)S	14.5
(5, 8, 3, 4)S	10.0
Nonuniform array	
U(5, 4, 1.5, 2)I and D(10, 8, 3, 2)I	10.1
U(5, 4, 3, 2)I and D(5, 8, 3, 2)I	9.9
U(5, 8, 3, 2)I and D(5, 4, 3, 2)I	9.9
U(10, 8, 3, 2)I and D(10, 4, 3, 2)I	10.4
U(10, 8, 6, 2)I and D(5, 4, 3, 2)I	10.1

† See also Fig. 1. In addition to being the streamwise separation between transverse jet rows, x_n/d is also the nondimensional width of the test plate segments. Thus experimental values of $Nu(x^+)$ represent averages over a streamwise distance of x_n/d. Since heat fluxes under the jet array exhibit sharp spatial variation, this averaging distance is significant there. Hence the value of x_n/d is always specified, even for geometries with $Nr = 1$.

TYPICAL TEST RUN

In keeping with the implication of equation (2) a typical test run consisted of three temperature levels. The first temperature level was attained by passing air through the test rig until the test surface achieved steady state adiabatic wall temperature. Usually it took $\frac{1}{2}$ to $1\frac{1}{2}$ h. Next, the temperatures of individual segments were raised to an isothermal level by supplying controlled power to their heaters through individual variacs. Usually it took $2\frac{1}{4}$ h to complete the first power level of a test run and $1–2\frac{1}{4}$ h for the second one. A temperature level was assumed to have attained steady state when average surface temperature changed by about 0.05 K or less over a few successive 5 min periods. The average value of temperature differences between adjacent segments were 0.07 K. The typical differences between surface and plenum temperatures were 17 and 25 K for lower and higher power levels, respectively.

DATA REDUCTION

Equation (2) averaged over one test plate segment yields

$$q(n) = h(n)[T_w(n) - T_r(n)] + \varepsilon(n) \quad (3)$$

where n refers to the segment number. Ideally $h(n)$ was to be determined from the slope of heat flux vs temperature difference curve fitted through at least two power runs. Operationally the heat transfer coefficients were calculated separately for each elevated surface temperature by using the following formula:

$$h(n) = \frac{q(n) - q^0(n)}{[T_w(n) - T_r(n)] - [T_w(n) - T_r(n)]^0} \quad (4)$$

where the superscript 0 refers to the zero power run. Even when no external power was supplied, differences in recovery effects over different segments and the consequent heat leakage between them occasionally made $q^0(n)$ larger than the experimental uncertainty in power input. Hence for all test runs $q^0(n)$ was routinely determined with energy balances based on calibrated segment-to-segment heat leaks. All nondimensional parameters were calculated independently for each temperature level, so that one could take into account the temperature dependent nature of fluid properties. The differences between magnitudes of different calculated variables, corresponding to the two temperature levels, were of the same order or less than the estimated experimental uncertainties (described below). This established the fact that equations (3) and (4) provided essentially equivalent results. Final Nusselt numbers reported were averages of results based on two different power input levels, except for five tests for which jet Reynolds numbers were low enough to neglect all high velocity effects so that only one heating level was used.

In determining each segment heat flux, corrections were applied to take into account the heat leaks from the back and ends of the segment and to adjacent segments. These were all modeled as steady state, constant property conduction.

In calculating the effective surface temperature, corrections were made to take into account the minute depressions in streamwise temperature distribution over the Lexan strips which were used to separate and insulate adjacent copper segments. An analytical solution of the steady state temperature field within the Lexan strip, subject to appropriate boundary conditions, was used for this purpose [19].

For segments under the jet array the jet exit total temperature, equivalent to the jet plenum static temperature, was used as the fluid reference temperature, T_r. For segments in the channel downstream of the jet array the reference temperature was taken to be the local mixed-mean temperature. In calculating local mixed-mean temperature over segment n, the gain in energy of the flowing air was assumed to be sum of all $q(m)$ upstream of segment n plus half of $q(n)$. The choice of reference temperature for locations immediately downstream of the jet array is not obvious, but the fact that the local mixed-mean temperature yields very cogent results (discussed later) suggests that it is an appropriate choice. The air flowing above the heated surface was at a higher temperature than that near side walls of the channel, giving rise to lateral diffusion of heat through the flow. The required correction for this was determined by measuring the spanwise distribution of centerline ($z^+ = 1/2$) air temperature at the channel exit. Its magnitude was of the order of 5% on each side. These measured values were taken to be representative for all streamwise locations ($x^+ > 0$). The corresponding corrections in local mixed-mean temperatures were incorporated in regular data reduction.

Since the channel width was larger than the width of the heat transfer surface (Fig. 2), the flow field above the heated surface was not affected by the side wall. In addition, the aspect ratio of the channel was quite large, ranging from 24 to 144. Therefore, the hydraulic diameter was assumed to be exactly $2z_n$. During calculation of nondimensional parameters temperature dependence of viscosity and thermal conductivity of air was taken into account. To account for any possible effect of variation of temperature dependent properties across the channel height, corrections were applied to the Nusselt number assuming $Nu \propto [T_w(n)/T_r(n)]^{-0.15}$, following recommendations of Sleicher and Rouse [20]. For details regarding analysis of different corrections and their typical magnitudes please refer to Sarkar [17].

The uncertainty associated with a single measurement was assumed to be equal to the least count of the measuring device or the band within which 95% or more of the repeated measurements fell, whichever was higher. For a detailed list of uncertainties associated with raw measurements please refer to Sarkar [17]. The composite uncertainty of a calculated quantity was determined by the method of Kline and McClintock [21]. Overall uncertainties for channel Reynolds number varied from ± 2 to $\pm 5\%$, and that for Nusselt number varied from ± 3 to $\pm 8\%$. Higher uncertainties in Nusselt number were observed near the end of the channel due to higher relative uncertainties in mixed-mean temperature and back heat leak. Also experiments at lower Reynolds numbers gave rise to higher relative uncertainties. In the figures in the following section the magnitude of Nusselt number uncertainties are indicated by vertical bars whenever they exceed the size of the data point symbols.

EXPERIMENTAL RESULTS

To study the effects of different parameters, each was varied over the desired range while keeping others constant. The nature of the dependence of $Nu(x^+)$ on these parameters precluded the possibility of a more economical experimental design.

Effect of Reynolds number

The effect of Re was investigated by studying $Nu(x^+)/Nu_\infty$ plots. Figure 4 shows the case of (10, 4, 3, 5)I geometry for Re varying from 10^4 to

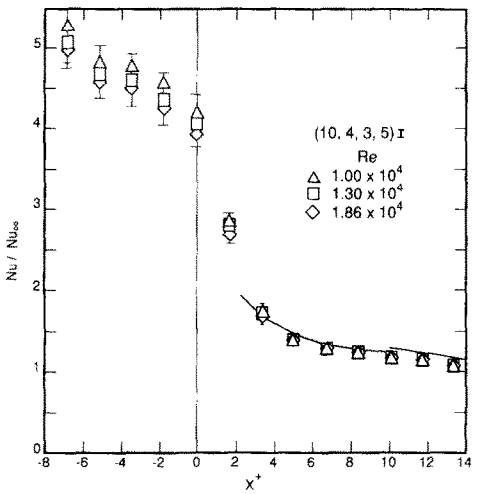

FIG. 4. Effect of Reynolds number. Solid curves represent empirical correlation, equations (5) and (6). ($V_c/V_j \approx 0.26$.)

1.86×10^4. Figure 5 shows the case of (5, 8, 1, 1)I geometry for Re of 3×10^3 and 8×10^3. For both cases $Nu(x^+)/Nu_\infty$ plots are independent of Re in the channel. For these plots $Nu_\infty = 0.0191 Re^{0.8}$, the fit from equation (7), was used. The effect of Reynolds number on turbulent entrance region heat transfer was investigated numerically by Deissler [22], Kays and Leung [23] and Leckner [24], and experimentally by Mills [25] and Tan and Charters [26]. Overall, these studies cover a wide range of Reynolds numbers, entrance geometries and thermal boundary conditions. In each case it was found that for turbulent flows $Nu(x^+)/Nu_\infty$ was not significantly affected by Re. In view of such strong support from literature, results of the above two data sets were deemed sufficient to draw the same conclusion in the present context.

From Figs. 4 and 5 it may be seen that $Nu(x^+)/Nu_x$ is not independent of Re under the jet array. Florschuetz *et al.* [4] found that for jet array impingement $Nu \propto Re_j^{0.73}$. These observations are in agreement with the present experiments.

Effects of geometry

Effects of geometry on Nusselt number are presented for a fixed channel Reynolds number of 10^4. To accomplish this small adjustments in Nusselt numbers from original data sets, where necessary, were based on an $Re^{0.8}$ dependence.

Effect of x_n/d. The effect of x_n/d was studied for three different basic geometries: $(x_n/d, 4, 3, 4)$I, $(x_n/d, 8, 1, 4)$I and $(x_n/d, 8, 3, 4)$I with $x_n/d = 5$ and 10. Representative results are shown in Fig. 6. It can be seen that in the channel, within the limits of experimental uncertainties, x_n/d does not have any influence on $Nu(x^+)$. This may be explained by the fact that none of the transverse averaged flow parameters at the channel entrance, e.g. jet exit velocity and the velocity of crossflow due to upstream jet rows, depend upon x_n/d. So in the channel $Nu(x^+)$ will not be a strong function of x_n/d unless it has a strong influence on the transverse and depthwise velocity and temperature profiles at the entrance of the channel, which is apparently not the case. The decrease in $Nu(x^+)$, under the jet array, with increase in x_n/d is consistent with observations of Florschuetz *et al.* [4].

Effect of y_n/d. The effect of y_n/d was studied for five different basic geometries: $(5, y_n/d, 1, 1)$I, $(5, y_n/d, 1, 4)$I, $(5, y_n/d, 3, 1)$I, $(5, y_n/d, 3, 4)$I and $(10, y_n/d, 3, 4)$I for $y_n/d = 4$ and 8. Two of the typical plots are shown in Figs. 7 and 8. All of these results show that increasing y_n/d increases $Nu(x^+)$ at the entrance region. The effect of change in y_n/d was more spectacular for higher values of z_n/d, i.e. when the influence of cross flow due to upstream spent air was less. Further discussion on the effect of V_c will follow. The effect of y_n/d became insignificant by 5–10

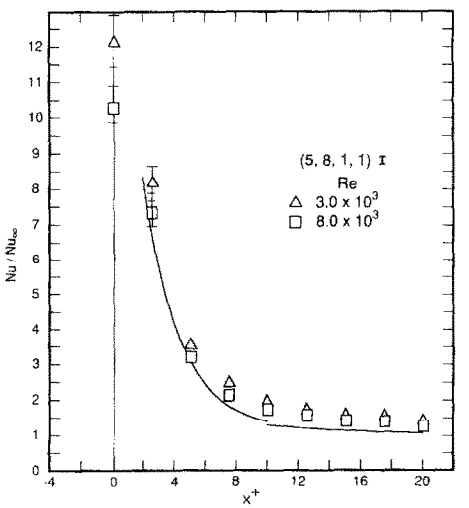

FIG. 5. Effect of Reynolds number. Solid curves represent empirical correlation, equations (5) and (6). ($V_c/V_j = 0$.)

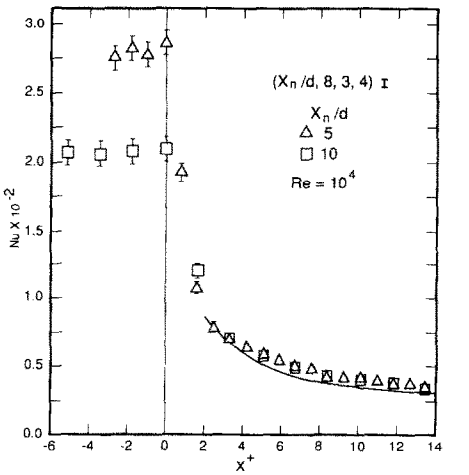

FIG. 6. Effect of x_n/d. Solid curves represent empirical correlation, equations (5) and (6). ($V_c/V_j \approx 0.10$, $Re_j = 1.3 \times 10^4$.)

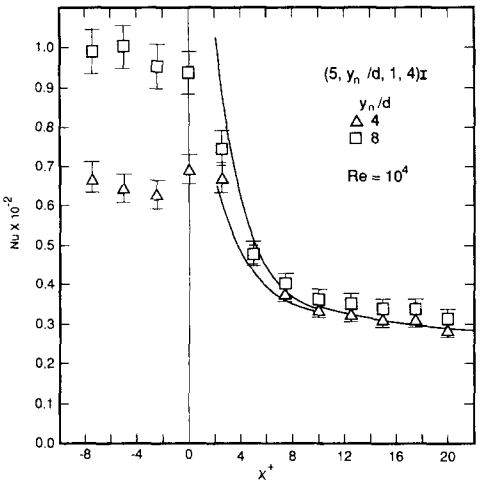

FIG. 7. Effect of y_n/d, for $z_n/d = 1$. Solid curves represent empirical correlation, equations (5) and (6). ($Re_j = 6.5 \times 10^3$ and 1.3×10^4, and $V_c/V_j \approx 0.59$ and 0.29 for $y_n/d = 4$ and 8, respectively.)

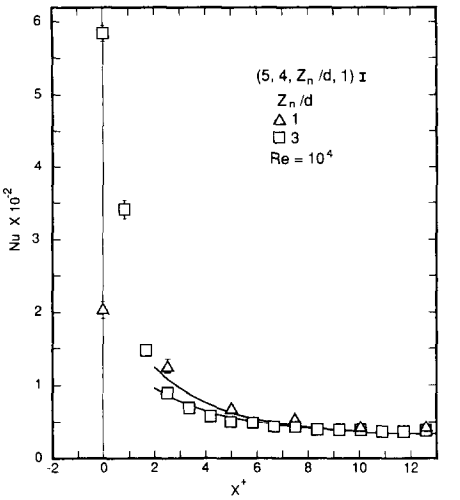

FIG. 9. Effect of z_n/d in the absence of crossflow due to upstream jet rows. Solid curves represent empirical correlations, equations (5) and (6). ($Re_j = 2.6 \times 10^4$ and $V_c/V_j = 0$.)

hydraulic diameters from the entrance. It can be deduced that the jet Reynolds number is proportional to $(y_n/d)/Nr$; hence increasing y_n/d tends to increase the heat flux at the entrance. This effect apparently overcomes the opposing effect on heat flux caused by the fact that impingement surface area per jet is proportional to y_n/d.

Effect of z_n/d. The effect of z_n/d was studied for five different basic geometries: $(5, 4, z_n/d, 1)$I, $(5, 8, z_n/d, 1)$I, $(5, 8, z_n/d, 4)$I and $(10, 4, z_n/d, 1)$I with $z_n/d = 1$ and 3; and $(10, 8, z_n/d, 4)$I with $z_n/d = 1$, 3 and 6. In Figs. 9–11 it may be seen that under the jet array, $Nu(x^+)$ is almost directly proportional to z_n/d. This is consistent with observations of Florschuetz *et al.* [4] and Sparrow *et al.* [13].

In Fig. 9 it is clear that increasing z_n/d from 1 to 3 decreases Nu in the channel entrance region. The same was true for all three cases with only one jet row. In Fig. 10 the effect of varying z_n/d is the opposite. In Fig. 11 it is seen that increasing z_n/d from 1 to 3 increases $Nu(x^+)$ at the entrance region, but further increase reverses the trend. This apparently complicated dependence on z_n/d may be explained by the following hypothesis: when the crossflow originating from upstream jet rows is weak compared to the jet exit velocity of the last row, the transverse averaged velocity profile at the channel entrance is similar to that of a wall jet. This is equivalent to the reasonable assumption that the transverse averaged velocity field created by a row of round jets is similar to a single transverse slot jet. Now $V_c/V_j \simeq (\pi/4)(Nr-1)/[(y_n/d)(z_n/d)]$. Hence when $Nr = 1$, e.g. in Fig. 9, or $Nr \ll (y_n/d)(z_n/d)$ (e.g. for higher z_n/d values in Fig. 11) the entrance region flow should be similar to a

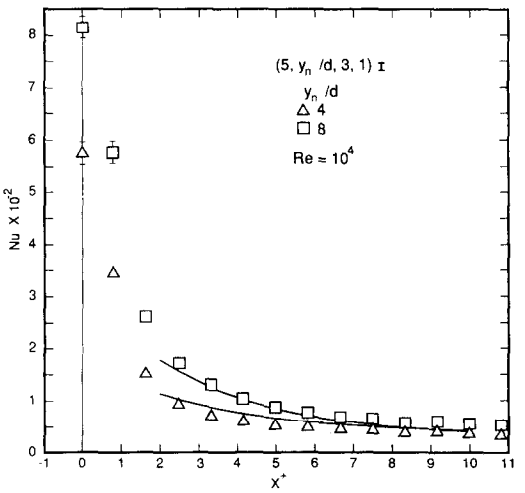

FIG. 8. Effect of y_n/d, for $z_n/d = 3$. Solid curves represent empirical correlation, equation (5). ($Re_j = 2.6 \times 10^4$ and 5.1×10^4 for $y_n/d = 4$ and 8, respectively; $V_c/V_j = 0$.)

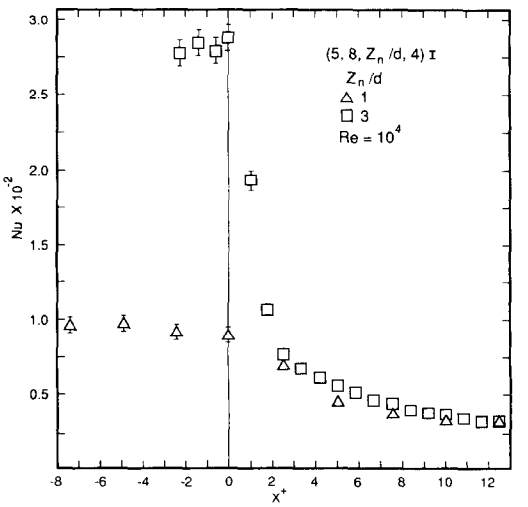

FIG. 10. Effect of z_n/d, when $V_c/V_j \neq 0$. ($V_c/V_j \approx 0.29$ and 0.1 for $z_n/d = 1$ and 3, respectively. $Re_j = 1.3 \times 10^4$.)

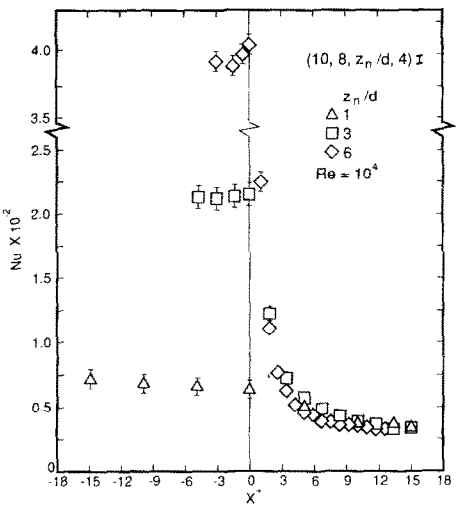

FIG. 11. Effect of z_n/d as V_c/V_j varies from 0.05 ($z_n/d = 6$) to 0.029 ($z_n/d = 1$). ($Re_j = 1.3 \times 10^4$.)

wall jet. Now for wall jets, $h \propto V_j^{0.75}(z_n/d)^{-0.35}x^{-0.6}$ (following Seban and Back [27]), explaining the decrease in Nu with increasing (z_n/d). For the present problem the least square data fit gives $Nu(x^+) \propto (z_n/d)^{-0.403}$, equation (5), compared to $Nu(x^+) \propto (z_n/d)^{-0.35}$ for a wall jet, putting further faith in the above hypothesis. When V_c/V_j is of order one increasing z_n/d, for the same Re, implies increasing Re_j; hence the accompanying increase in $Nu(x^+)$. For $x^+ \geqslant 10$, changes in the values of $Nu(x^+)$ observed by varying z_n/d are of the same order as experimental uncertainties or less.

Effect of number of rows. Effects of varying Nr were studied for five different geometries: $(10, 4, 3, Nr)$I with $Nr = 1, 2, 4, 5$; $(5, 4, 1, Nr)$I with $Nr = 1, 2, 4$; $(5, 4, 3, Nr)$I, $(5, 8, 1, Nr)$I and $(5, 8, 3, Nr)$I with $Nr = 1$ and 4. Two of these are shown in Figs. 12 and

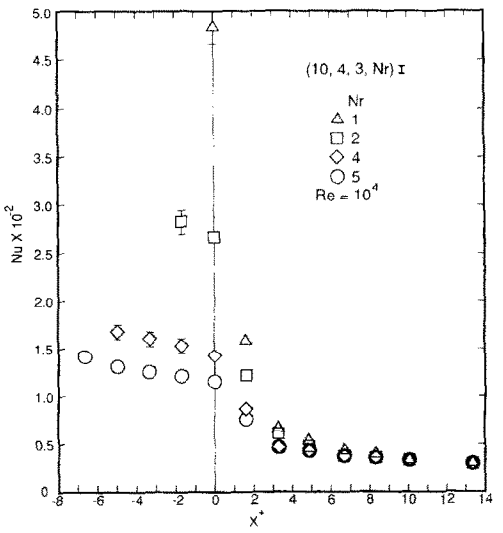

FIG. 12. Effect of number of transverse jet rows. (Re_j decreases from 2.1×10^4 to 0.52×10^4, and V_c/V_j increases from 0 to 0.26 as Nr increases from 1 to 5.)

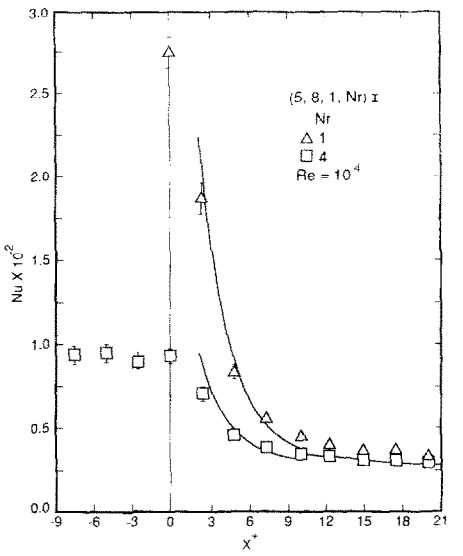

FIG. 13. Effect of number of jet rows. Solid curves represent empirical correlation, equations (5) and (6). ($Re_j = 5.1 \times 10^4$ and 1.3×10^4, and $V_c/V_j = 0$ and 0.29 for $Nr = 1$ and 4, respectively.)

13. The $Nu(x^+)$ under the jet array is consistent with earlier observations of Florschuetz *et al.* [4]. It can be seen that, downstream of the jet array, decreasing Nr increases $Nu(x^+)$ regardless of values of other parameters. It can be shown that $Re_j \propto (y_n/d)/Nr$, hence reducing Nr increases the heat fluxes at the channel entrance. As Nr is increased, the crossflow due to the spent air of upstream rows tends to reduce the heat fluxes even further. See Florschuetz *et al.* [9] and Florschuetz and Su [10] for detailed studies of the effect of crossflow within a jet array. The present results show that the effect of Nr on $Nu(x^+)$ becomes negligible by 5–12 hydraulic diameters from the channel entrance.

Effect of jet array pattern. The effect of jet array pattern, i.e. inline or staggered (Fig. 1), was studied for three basic geometries: (5, 4, 3, 4), (5, 8, 2, 2) and (5, 8, 3, 4). Figure 14 shows a typical plot. Under the jet array the effect of array pattern is appreciable, as was observed in earlier studies of Florschuetz *et al.* [4]. But downstream of the jet array it does not have any recognizable effect. This may be explained by the fact that transverse averaged flow quantities at the channel entrance are independent of the array pattern. Whatever effect the array pattern might have had on the transverse distribution of these quantities, it was not significant enough to give rise to any difference in the transverse average heat transfer coefficients. It may be noted that the effect of x_n/d was similar.

Nonuniform jet arrays. A total of five nonuniform geometries were tested (Table 1). The arrays were limited to a total of four transverse jet rows. Two of these are shown, along with the corresponding inline geometry results, in Figs. 15 and 16, in which y_n/d and the jet hole diameters are varied across the jet array respectively. For the case in Fig. 15 the uniform array

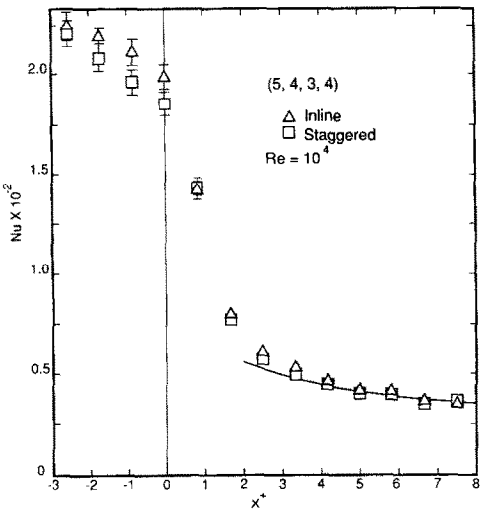

FIG. 14. Effect of jet array pattern. Solid curve represents empirical correlation, equation (5). ($Re_j \approx 6.5 \times 10^3$ and $V_c/V_j \approx 0.2$.)

gives higher heat transfer rates at the channel entrance. This may be explained as follows. For this case, the jet exit velocity, V_j, will be nearly the same in all the transverse rows [5]. Because of larger transverse spacing the uniform geometry jet plate has only two-thirds as many jet holes as the nonuniform geometry, hence for the same Re, correspondingly higher V_j and higher heat fluxes downstream of the jet array. The sharp variation in $Nu(x^+)$ under the jet array for the nonuniform geometry is because of the change in the average heat transfer surface area per impinging jet (but not Re_j) for different transverse rows. Explanation of the comparisons in Fig. 16 is almost identical.

Behavior of all other nonuniform array results can be similarly explained, case by case. The general conclusion is that heat transfer at the entrance region of the channel is most sensitive to the cross flow to jet exit velocity ratio at the last transverse row and to the jet Reynolds number. The influence of geometry of the jet array is felt mainly through the way it affects these two flow parameters.

Empirical correlations

Entrance region. Theoretical solutions of thermal entrance lengths give rise to an infinite number of exponentially decreasing eigenfunctions. This suggested including exponential functions in the correlations, with possible dependence of exponents on geometric parameters. Theoretically these exponents should also depend upon Re, but based on experimental evidence this possibility was neglected. A correlation of this type should asymptotically yield the fully developed Nusselt number, so a term in the form of the Dittus–Boelter equation was also included. Attempts were made to develop correlations in terms of flow parameters (e.g. Re_j, V_c/V_j) instead of the geometry, so that the correlation may have wider applicability. Results of these attempts were less than satisfactory. A simple power law dependence on geometric parameters worked best. This is consistent with the observations of Florschuetz *et al.* [4] that different combinations of geometries, corresponding to the same V_c/V_j and Re_j, give rise to significant different heat fluxes under the jet array. Therefore, V_c/V_j and/or Re_j were not used as independent parameters in correlating the present experimental results.

It turned out to be simpler to use one correlation for $x^+ \leqslant 10.0$ and another for $x^+ > 10.0$. The latter turned out to be practically independent of all geometric parameters. There are very few data points for the region $0 < x^+ < 2.0$. Also, in this region the flow is expected to be closer to a stagnation flow than a wall jet or channel flow, which is different from the rest of the channel. Hence the correlation was developed for $x^+ \geqslant 2.0$.

The following are the final least square fit to the available experimental points.

For $2.0 \leqslant x^+ \leqslant 10.0$

$$Nu(x^+) = 0.0236 Re^{0.8} Pr^{0.4} Nr^{-0.715} (y_n/d)^{1.26} \times (z_n/d)^{-0.403} \exp[-(0.295 + 0.0169(y_n/z_n))x^+] + 0.0225 Re^{0.8} Pr^{0.4}. \quad (5)$$

For $x^+ > 10.0$

$$Nu(x^+) = 0.0279 Re^{0.8} Pr^{0.4} \exp[-0.161 x^+] + 0.019 Re^{0.8} Pr^{0.4}. \quad (6)$$

The dependence on Pr was artificially introduced to conform to the form of the Dittus–Boelter equation. Pr was equal to 0.7 in all the test runs. Equation (5) is the least square fit to 139 data points. The average deviation of experimental points was 7.1%, with 72% of data points within $\pm 10\%$, 94% within $\pm 15\%$ and all within $\pm 20\%$ of the correlation, save one which deviated by 22%. The majority of the large deviations occurred for geometries with $z_n/d = 1$ and/or $Nr = 1$. Equation (6) is the least square fit to 290 data points, including those from nonuniform geometries (see Fig. 3 for definition of nonuniform geometry). Average deviations of data points were 7.0%; 75% fell within $\pm 10\%$, and 97% fell within $\pm 15\%$ of the correlation. Comparison of these equations with data can be seen in Figs. 4–9, 13 and 14.

To check the sensitivity of the correlation (5) to input data points, half of the data points were removed and a new least square fit developed. As a consequence the exponent of z_n/d changed by 30% and all other constants by less than 15%. When the new correlation, thus developed, was applied to all the 139 data points the average deviation was 10.6%, with a maximum deviation of 28.1%. This indicates the ability of the correlation to handle new data. No attempt was made to make the two correlations blend smoothly at $x^+ = 10.0$. The resulting discontinuities

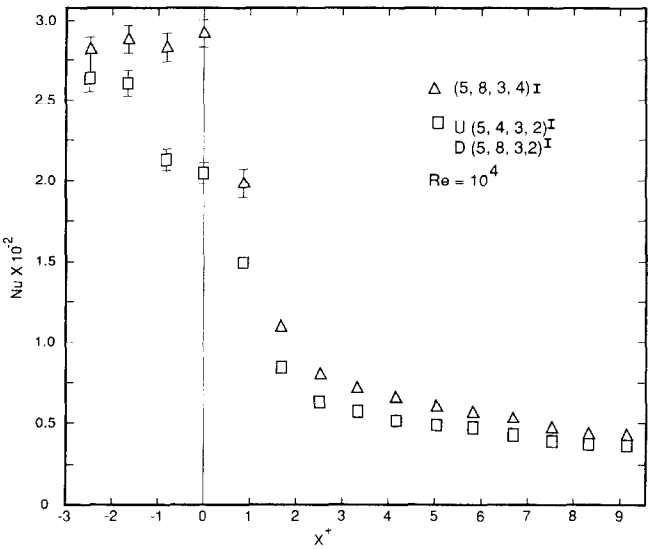

FIG. 15. Effect of nonuniform jet array pattern when y_n/d changes across the jet array. ($Re_j = 1.3 \times 10^4$ and 0.84×10^4, and $V_c/V_j \approx 0.1$ and 0.16 for the uniform and nonuniform arrays, respectively.)

in predicted values of Nusselt number were of the same order as the experimental uncertainties.

Entrance length. Figure 17 shows $Nu(x^+)/Nu_\infty$ vs x^+ plots, for $x^+ > 10.0$ and $Re \simeq 10^4$. No distinction is made between data from different jet array patterns, since the effect of most geometric parameters became negligible by $x^+ \simeq 10.0$. The smooth curve is the least square fits through original data points (equation (6)). According to this correlation it takes 21 hydraulic diameters for $Nu(x^+)$ to be within 5% of the fully developed value. This is larger than the value of 10–13 hydraulic diameters obtained by Sparrow and Cur [15], but less than the value of 60 reported by Tan and Charters [26], both for a straight duct with asymmetric heating. The present entrance length is of the same order as those observed downstream of a mixing tee [14, 29] and downstream of fluid withdrawal branches [31]. Although the spanwise averaged $Nu(x^+)$ was fully developed by $x^+ \simeq 21$, the spanwise distribution of channel air temperature measurements showed detectable periodicity, corresponding to the positions of streamwise jet columns, as far as $x^+ \simeq 40$. The amplitudes of these deviations were about 5% of the reference temperature difference.

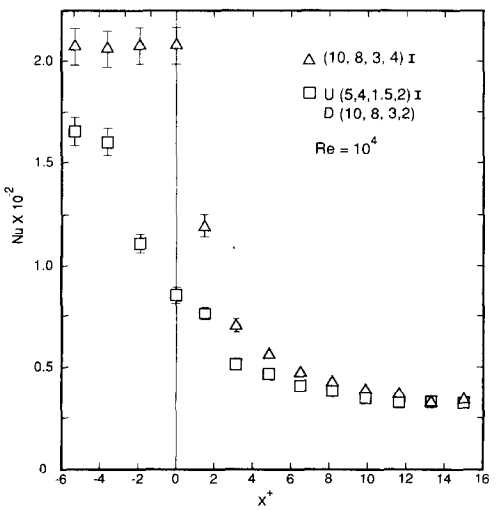

FIG. 16. Effect of nonuniform jet array pattern when jet hole diameter changes across the array. (Uniform array $Re_j = 1.3 \times 10^4$ and $V_c/V_j \approx 0.1$. Nonuniform array $V_c/V_j \approx 0.29$ and $Re_j = 0.52 \times 10^4$ at $x^+ = 0$.)

Fully developed flow. From equations (5) and (6) it is clear that in our case the fully developed value of Nusselt number is given by

$$Nu_\infty = 0.0191 Re^{0.8} Pr^{0.4}. \quad (7)$$

It is about 16% less than that of a symmetrically heated pipe (Petukhov [28]). This may be compared with the 20% decrease observed by Sparrow *et al.* [29] in a similar situation. Equation (7) is very close to the relationship, $Nu_\infty = 0.018 Re^{0.8} Pr^{0.4}$, proposed by Tan and Charters [30]. Numerical computations by Kays and Leung [23] are within 6% of equation (7) for Re from 10^4 to 10^6. In all these references the thermal boundary condition at the heated surface was that of constant heat flux, in present experiments it was constant temperature. Sparrow and Cur [15] proposed the following correlation based on mass transfer experiments in a parallel plate channel $Sh_x = 0.0464 Re^{0.76}$. The effective thermal boundary conditions in these experiments were that of one surface isothermal and the other adiabatic. They used naphthalene sublimation technique with air as the working fluid.

Figure 18 compares the present experimental data with equation (7) and other correlations and some of the data available in literature. Each of the experimental points in this figure represents the mean Nus-

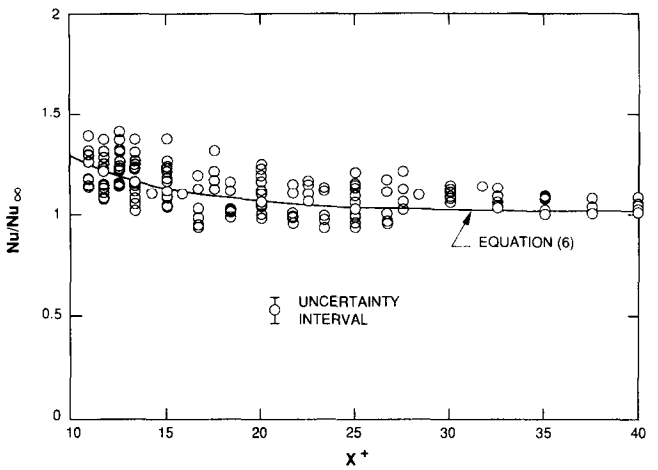

FIG. 17. Heat transfer rate variation far from the channel entrance. Data points are taken from all the jet array geometries with $Re \simeq 10^4$. The solid curve is from equation (6).

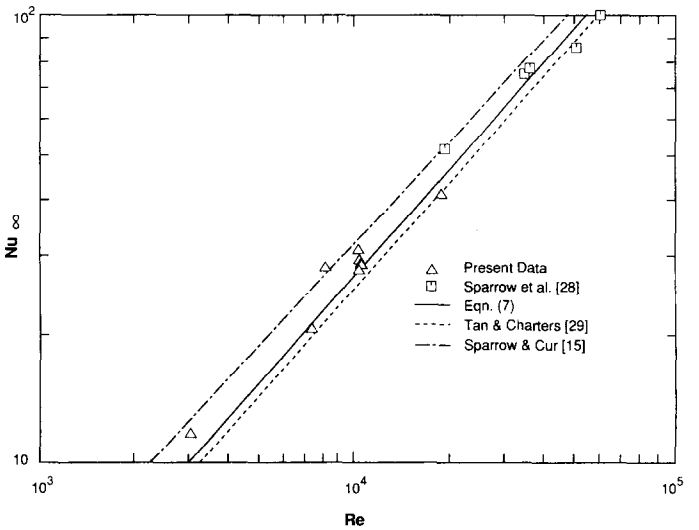

FIG. 18. Comparison of equation (7) and other correlations with experimental data from the present study and Sparrow *et al.* [29].

selt number averaged over all the heat transfer segments with $x^+ \geqslant 30$. The correlation of Sparrow and Cur [15] was modified assuming $Sh \propto Sc^{0.4}$, and for air $Sc = 2.39$ and $Pr = 0.7$. It is to be concluded that the present observations are consistent with other reported observations.

CONCLUSIONS

Heat transfer rates at the entrance region of a parallel plate channel, situated downstream of an impinging jet array (Fig. 1), were investigated experimentally. The working fluid was air. The impingement surface of the channel was maintained isothermal while the opposite surface was adiabatic. The major findings may be summarized as follows:

- In the channel $Nu(x^+)/Nu_\infty$ was independent of Re, within the limits of experimental uncertainties, for $3 \times 10^3 \leqslant Re \leqslant 18.6 \times 10^3$.
- The streamwise spacing of jet rows, x_n/d, had no detectable influence on $Nu(x^+)$ distribution in the channel.
- Increasing the spanwise spacing of jets, y_n/d, increased the Nusselt number both at the entrance region of the channel and under the jet array.
- When $Nr = 1$ or $Nr \ll (y_n/d)(z_n/d)$ increasing z_n/d reduced $Nu(x^+)$ at the entrance region. Otherwise $Nu(x^+)$ increased with increase in z_n/d.
- Increasing Nr decreases Re_j and increases V_c/V_j, and thus decreases $Nu(x^+)$ at the channel entrance.
- The jet array pattern, i.e. whether inline or staggered, did not noticeably influence the $Nu(x^+)$ distribution in the channel.
- The results with nonuniform geometries, the effect

of x_n/d and the effect of jet array pattern, taken together suggest that heat fluxes in the channel entrance region are most dependent upon the jet exit velocity and the crossflow to jet exit velocity ratio for the last spanwise row. The influence of the geometry of the jet array is felt mainly through the way they affect these flow parameters. $Nu(x^+)$ increases with increase in V_j and/or decrease in V_c/V_j.

- Effect of varying different geometric parameters on $Nu(x^+)$ became negligible by $x^+ \simeq 10$.
- $Nu(x^+)$ attained the fully developed value by $x^+ \simeq 21$.
- The fully developed Nusselt number at the heated surface was found to be 16% lower than that of a symmetrically heated channel.

It is to be remembered that all the above comments relate to transverse average values of $Nu(x^+)$

Acknowledgements—The lead author was financially supported through graduate assistantships, by the Mechanical and Aerospace Engineering Department, Arizona State University, during most of the present work. During preparation of the manuscript he was supported by an Office of Naval Research grant (N00014-84-K-0080) through the Johns Hopkins University.

REFERENCES

1. J. W. Gauntner, H. J. Gladen, D. J. Gauntner and F. C. Yeh, Crossflow effects on impingement cooling of a turbine vane, NASA TM X-3029 (1974).
2. E. P. Dyban, A. I. Mazur and V. P. Golovanov, Heat transfer and hydrodynamics of an array of round impinging jets with one-sided exhaust of the spent air, *Int. J. Heat Mass Transfer* **23,** 667–676 (1980).
3. L. W. Florschuetz, R. A. Berry and D. E. Metzger, Periodic streamwise variations of heat transfer coefficients for inline and staggered arrays of circular jets with crossflow of spent air, *J. Heat Transfer* **102,** 132–137 (1980).
4. L. W. Florschuetz, C. R. Truman and D. E. Metzger, Streamwise flow and heat transfer distributions for jet array impingement with crossflow, *J. Heat Transfer* **103,** 337–342 (1981).
5. L. W. Florschuetz and H. H. Tseng, Effects of non-uniform geometries on flow distribution and heat transfer characteristics for arrays of impinging jets, *J. Engng Gas Turbine Pwr* **107,** 68–75 (1985).
6. R. J. Goldstein and J. F. Timmers, Visualization of heat transfer from arrays of impinging jets, *Int. J. Heat Mass Transfer* **25,** 1857–1868 (1982).
7. D. M. Kercher and W. Tabakoff, Heat transfer by a square array of round air jets impinging perpendicular to a flat surface including the effect of spent air, *J. Engng Pwr* **92,** 73–82 (1970).
8. D. E. Metzger, L. W. Florschuetz, D. I. Takeuchi, R. D. Behee and R. A. Berry, Heat transfer characteristics for inline and staggered arrays of circular jets with crossflow of spent air, *J. Heat Transfer* **101,** 526–531 (1979).
9. L. W. Florschuetz, D. E. Metzger and C. C. Su, Heat transfer characteristics for jet array impingement with initial crossflow, *J. Heat Transfer* **106,** 34–41 (1984).
10. L. W. Florschuetz and C. C. Su, Effects of crossflow temperature on heat transfer within an array of impinging jets, *J. Heat Transfer* **109,** 74–82 (1987).
11. J. P. Bouchez and R. J. Goldstein, Impingement cooling from a circular jet in a crossflow, *Int. J. Heat Mass Transfer* **18,** 719–730 (1975).
12. J. W. Ramsey and R. J. Goldstein, Interaction of a heated jet with a deflecting stream, *J. Heat Transfer* **93,** 365–372 (1971).
13. E. M. Sparrow, R. J. Goldstein and M. A. Rouf, Effect of nozzle-surface separation distance on impingement heat transfer for a jet in a crossflow, *J. Heat Transfer* **97,** 528–533 (1975).
14. E. M. Sparrow and R. G. Kemink, The effect of a mixing tee on turbulent heat transfer in a tube, *Int. J. Heat Mass Transfer* **22,** 909–917 (1979).
15. E. M. Sparrow and N. Cur, Turbulent heat transfer in a symmetrically or asymmetrically heated flat rectangular duct with flow separation at inlet, *J. Heat Transfer* **104,** 82–89 (1982).
16. R. J. Goldstein and A. I. Behbahani, Impingement of a circular jet with or without crossflow, *Int. J. Heat Mass Transfer* **25,** 1377–1382 (1982).
17. A. Sarkar, Entrance region heat transfer in a parallel plate channel downstream of arrays of impinging jets, M.S. Thesis, Arizona State University, Tempe, Arizona (1986).
18. E. R. G. Eckert and R. M. Drake, Jr., *Analysis of Heat and Mass Transfer*, Chapter 10. McGraw-Hill, New York (1972).
19. L. W. Florschuetz, D. E. Metzger, D. I. Takeuchi and R. A. Berry, Multiple jet impingement heat transfer characteristics—experimental investigation of inline and staggered arrays with crossflow. NASA Contractor Report, NASA CR-3217 (1980).
20. C. A. Sleicher and M. W. Rouse, A convenient correlation for heat transfer to constant and variable property fluids on turbulent pipe flow, *Int. J. Heat Mass Transfer* **18,** 677–683 (1975).
21. S. J. Kline and F. McClintock, Describing uncertainties in single sample experiments, *Mech. Engng* **75,** 3–8 (1953).
22. R. G. Deissler, Turbulent heat transfer and friction in the entrance region of smooth passages, *Trans. ASME* **77,** 1221–1223 (1955).
23. W. M. Kays and E. Y. Leung, Heat transfer in annular passages—hydrodynamically developed turbulent flow with arbitrarily prescribed heat flux, *Int. J. Heat Mass Transfer* **6,** 537–557 (1963).
24. B. Leckner, Heat transfer in the entrance region with fully developed turbulent flow between parallel plates, *Int. J. Heat Mass Transfer* **15,** 35–42 (1972).
25. A. F. Mills, Experimental investigation of turbulent heat transfer in the entrance region of a circular conduit, *J. Mech. Engng Sci.* **4,** 63–77 (1962).
26. H. M. Tan and W. W. S. Charters, Effect of thermal entrance region on turbulent forced-convective heat transfer for an asymmetrically heated rectangular duct with uniform heat flux, *Solar Energy* **12,** 513–516 (1969).
27. R. A. Seban and L. H. Back, Velocity and temperature profiles in a wall jet, *Int. J. Heat Mass Transfer* **3,** 255–265 (1961).
28. B. S. Petukhov, Heat transfer and friction in turbulent pipe flow with variable physical properties, *Adv. Heat Transfer* **6,** 503–564 (1970).
29. E. M. Sparrow, J. R. Lloyd and C. W. Hixon, Experiments on turbulent heat transfer in an asymmetrically heated rectangular duct, *J. Heat Transfer* **88,** 170–174 (1966).
30. H. M. Tan and W. W. S. Charters, An experimental investigation of forced-convective heat transfer for fully-developed turbulent flow in a rectangular duct with asymmetric heating, *Solar Energy* **13,** 121–125 (1970).
31. E. M. Sparrow and R. G. Kemink, Heat transfer downstream of a fluid withdrawal branch in a tube, *J. Heat Transfer* **101,** 23–28 (1979).